Thermal regime of the Southeast Indian Ridge between 88°E and 140°E: Remarks on the subsidence of the ridge flanks

L. Géli, J. R. Cochran, T. C. Lee, J. Francheteau, C. Labails, C. Fouchet, D. Christie

JOURNAL OF GEOPHYSICAL RESEARCH, VOL. 112, B10101, doi:10.1029/2006JB004578, 2007

Thermal regime of the Southeast Indian Ridge between 88°E and 140°E: Remarks on the subsidence of the ridge flanks

L. Géli,[1] J. R. Cochran,[2] T. C. Lee,[3] J. Francheteau,[4] C. Labails,[1] C. Fouchet,[1] and D. Christie[5]

Received 16 June 2006; revised 13 February 2007; accepted 1 June 2007; published 5 October 2007.

[1] The flanks of the Southeast Indian Ridge are characterized by anomalously low subsidence rates for the 0–25 Ma period: less than 300 m $Ma^{-1/2}$ between 101°E and 120°E and less than 260 m $Ma^{-1/2}$ within the Australian-Antarctic Discordance (AAD), between 120°E and 128°E. The expected along-axis variation in mantle temperature (~50°C) is too small to explain this observation, even when the temperature dependence of the mantle physical properties is accounted for. We successively analyze the effect on subsidence of different factors, such as variations in crustal thickness; the dynamic contribution of an old, detached slab supposedly present within the mantle below the AAD; and depletion in φ_m, a parameter here defined as the ''ubiquitously distributed melt fraction'' within the asthenosphere. These effects may all contribute to the observed, anomalously low subsidence rate of the ridge flanks, with the most significant contribution being probably related to the depletion in φ_m. However, these effects have a deep-seated origin that cannot explain the abruptness of the transition across the fracture zones that delineate the boundaries of the AAD, near 120°E and near 128°E, respectively.

Citation: Géli, L., J. R. Cochran, T. C. Lee, J. Francheteau, C. Labails, C. Fouchet, and D. Christie (2007), Thermal regime of the Southeast Indian Ridge between 88°E and 140°E: Remarks on the subsidence of the ridge flanks, *J. Geophys. Res.*, *112*, B10101, doi:10.1029/2006JB004578.

1. Introduction

[2] Between the Saint Paul/Amsterdam Islands and the western boundary of the Australian-Antarctic Discordance, the axial seafloor of the Southeast Indian Ridge (Figure 1) deepens by more than 2000 m [e.g., *Cochran et al.*, 1997; *Sempéré et al.*, 1997]. The ridge flank depth (right next to the axis) increases by ~500 m [*Ma and Cochran*, 1997], the axial crust thickness decreases by more than ~3 km [e.g., *Tolstoy et al.*, 2002; *Kojima et al.*, 2003; *Holmes et al.*, 2005], the crestal morphology changes from an axial high to a pronounced axial valley [e.g., *Small et al.*, 1999], and the basalt geochemistry displays significant variations [e.g., *Klein et al.*, 1988; *Mahoney et al.*, 2002]. Because the spreading rate remains almost constant (the total rate only varies from 68 km Ma^{-1} near the Rodriguez Triple Junction to 76 km Ma^{-1} near 140°E), these variations have primarily been ascribed to variations in mantle temperature [e.g., *Shah and Sempére*, 1998].

[3] In this paper, we first review the different estimates that have been proposed for mantle temperature variations beneath the Southeast Indian Ridge. All observational evidence (based on bathymetry, seafloor morphology, crustal thickness and basalt geochemistry) suggest that the along-axis temperature variation does not exceed ~50°C. Then, we examine the subsidence rate of the ridge flanks, a first-order proxy of mantle temperature variations. As found by previous workers [e.g., *Cochran*, 1986; *Kane and Hayes*, 1994; *Sykes*, 1995], we find that the expected along-axis changes in mantle temperature are too small to explain the subsidence rate of the ridge flanks, which have long been known to be anomalously low. Other possible effects are hence reviewed.

2. Geological and Geophysical Setting

[4] Seafloor spreading at the Southeast Indian Ridge (SEIR) started during late Cretaceous [e.g., *Cande and Mutter* [1982]; *Tikku and Cande* [1999]. Until mid-Eocene, spreading was very slow (<10 km Ma^{-1}) and oblique. After about Chron 20 (~43 Ma), spreading was established at an intermediate rate, with no significant change in characteristics (direction and rate) during the last 36 Ma [*Royer and Sandwell*, 1989], except within the AAD, where kinematics events have been documented during Miocene time [*Marks et al.*, 1999].

[5] Near 78°E, the SEIR is influenced by the presence of the Amsterdam and Saint Paul (ASP) Islands which sit on the Antarctic plate, less than 40 km away from the spread-

[1]Marine Geosciences Department, Ifremer, Plouzané, France.
[2]Lamont Doherty Geological Observatory of Columbia University, Palisades, New York, USA.
[3]College of Ocean and Atmospheric Sciences, Oregon State University, Corvallis, Oregon, USA.
[4]Université de Bretagne Occidentale, UMR CNRS 6538, Plouzané, France.
[5]West Coast and Polar Regions Undersea Research Center, University of Alaska Fairbanks, Fairbanks, Alaska, USA.

0148-0227/07/2006JB004578$09.00

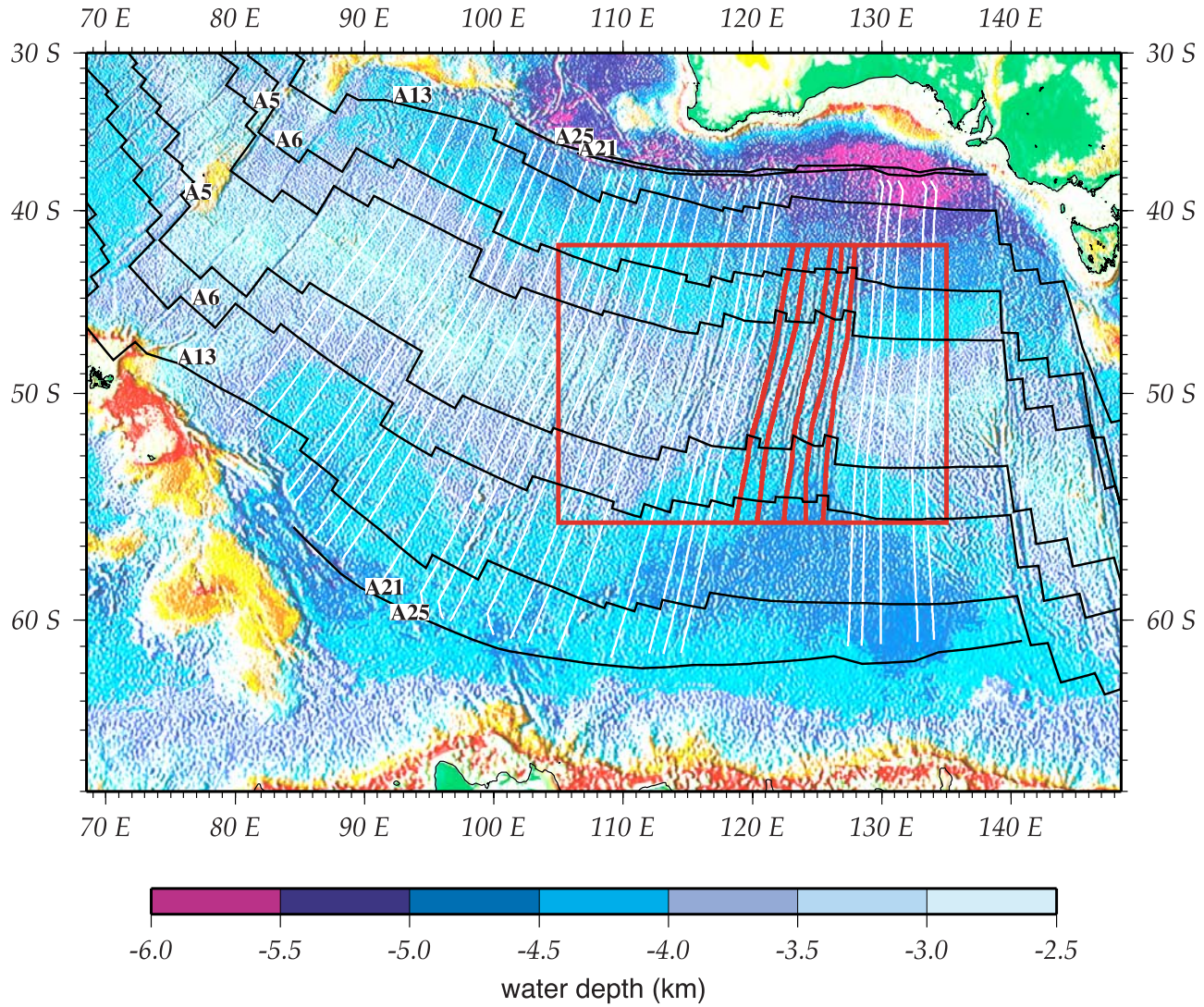

Figure 1. Satellite-derived bathymetry map of the study area [*Smith and Sandwell*, 1997]. White lines across the Southeast Indian Ridge indicate synthetic flow lines used to reassess the subsidence rate pattern. Flow lines crossing the SEIR between 120°E and 128°E (red lines) are based on the plate kinematics parameters (rotation poles and angles) of *Marks et al.* [1999]. Elsewhere, poles by *Royer and Sandwell* [1989] are used (thin, white lines). Flow lines were carefully selected so as to avoid structural effects, such as fracture zones, off-axis seamounts, intraplate volcanism, propagators trails. Although Australia and Antarctica began to drift apart during the Upper Cretaceous, spreading rates were ultraslow until late Eocene times, so that only those subsidence rates computed for ages younger than 42 Ma are significant for regional geodynamic studies of the physiographic domain extending from the ridge crest to the foot of the continental slope. Here we examine subsidence rates for the 0–25 Ma period, after the onset of the AAD-related fracture zones [*Marks et al.*, 1999].

ing center [*Scheirer et al.*, 2000]. As the ASP hot spot was captured by the SEIR, about 3.5 Ma ago, excess volcanism formed a plateau of ~150 × 200 km^2, which stands 1 to 3 km above the surrounding seafloor. The influence of the ASP is thus relatively localized compared to that of the more distant but larger Kerguelen hot spot. Although it is located more than about 1100 km from the nearest SEIR segment, the Kerguelen anomaly influences the ridge axial depth and morphology over distances of several thousands of kilometers [*Small*, 1995; *Ma and Cochran*, 1997].

[6] Between ~118°E and 128°E (Figure 2), the Australian-Antarctic Discordance (AAD) was first recognized as a region of rough topography and deep regional bathymetry [*Hayes and Conolly*, 1972] centered on the Southeast Indian Ridge. It was proposed that it represents the surface expression of regionally cooler mantle temperatures [*Weissel and Hayes*, 1974]. The AAD is located in the center of a depth anomaly that extends from Antarctica to Australia [e.g., *Marks et al.*, 1990] that persisted at least over the last 100 Ma [e.g., *Veevers*, 1982; *Gurnis et al.*, 1998]. The AAD thus appears to be related to a long-term mantle anomaly,

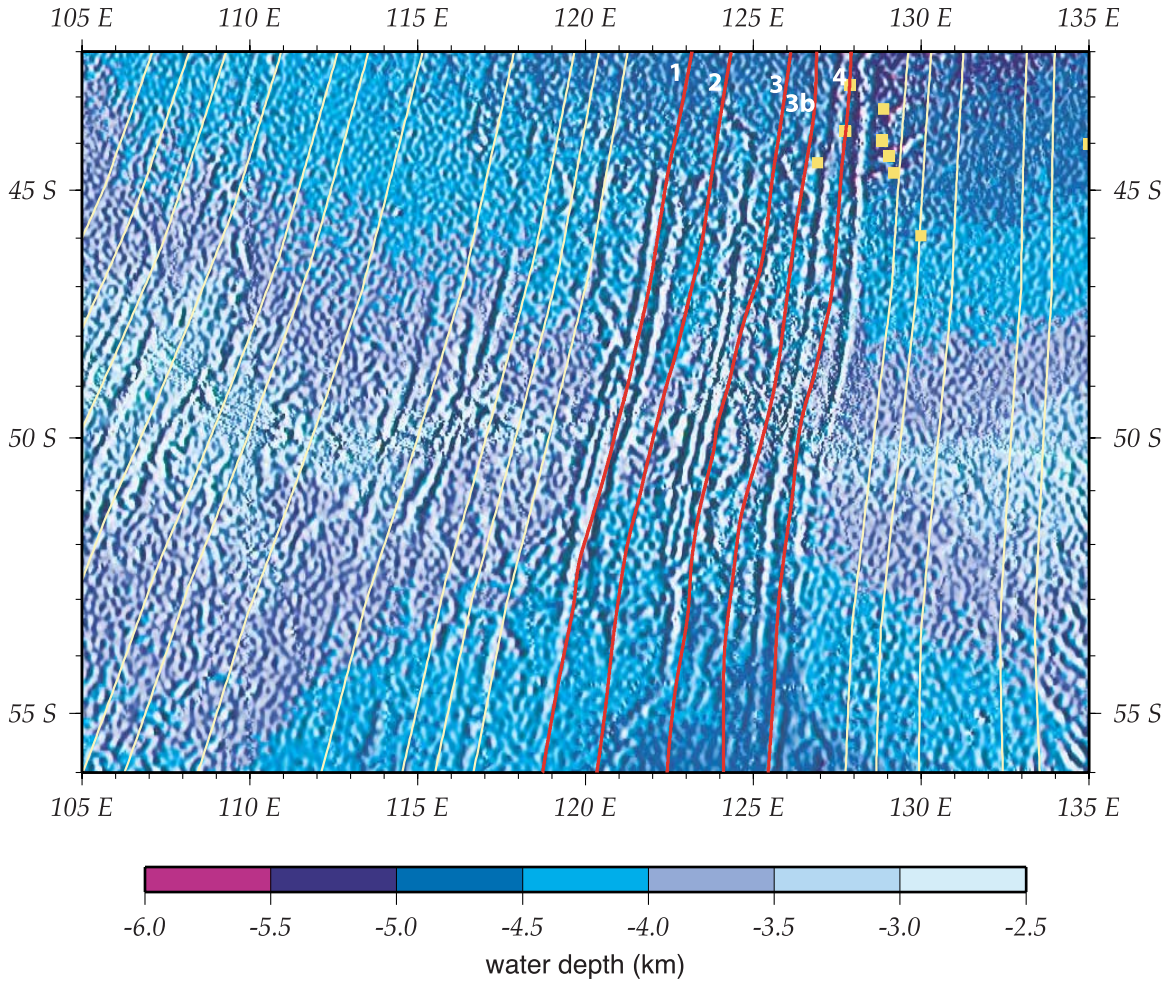

Figure 2. Close-up of seafloor bathymetry within the AAD. Red lines indicate flow lines after *Marks et al.* [1999], numbered 1, 2, 3, 3b, and 4. Note that the subsidence averages (see text) between 120°E and 128°E have been computed without flow line 1. White flow lines are based on the work by *Royer and Sandwell* [1989]. Yellow squares indicate ODP Leg 187 drilling sites [*Christie et al.*, 2004].

the surface expression of which evolves through time, as evidenced by the fact that rough seafloor topography and fracture zone offsets in the AAD have increased, about 30–25 Ma ago [e.g., *Weissel and Hayes*, 1974; *Vogt et al.*, 1983; *Christie et al.*, 1998; *Okino et al.*, 2004].

[7] Early seismological work [e.g., *Montagner*, 1986; *Forsyth et al.*, 1987; *Kuo*, 1993; *Roult et al.*, 1994] indicated the presence of high seismic mantle velocities below the AAD. *Gurnis and Müller* [2003] have reviewed results from three different global seismic inversion models at three different depths (100, 400, and 900 km): model SB4L18 [*Masters et al.*, 2000]; SAW24B16 [*Megnin and Romanowicz*, 2000]; and S20RTS [*Ritsema and van Heijst*, 2000]. Although the horizontal resolution is >1000 km, all three models show a north-south trending high shear wave velocity anomaly in the lower mantle and near the transition zone (670 km) beneath the AAD. Using broadband surface wave group and phase velocity measurements, *Ritzwoller et al.* [2003] have recently resolved a NW-SE trending anomaly (Figure 3), termed as the Australian-Antarctic Mantle Anomaly (AAMA). On the basis of surface wave tomography, the depth extent of the AAMA appears to be confined to the upper ~120 km of mantle [*Ritzwoller et al.*, 2003].

3. Estimates of Mantle Temperature Variations Beneath the Southeast Indian Ridge

[8] From melting models [e.g., *McKenzie*, 1984] and from models on the formation of axial topography [e.g., *Chen and Morgan*, 1990], it can be inferred that the observed contrasts in axial depth and morphology along the SEIR require thicker crust and warmer upper mantle temperatures both to the east and west of the AAD. This prediction is confirmed by direct measurements based on OBS data from different segments of the SEIR. Within the AAD, thin crustal thicknesses of 3.6 km and of 4.2 km have been measured, respectively, near 125°E [*Kojima et al.*, 2003] and near ~127 and ~128°E [*Tolstoy et al.*, 2002]. In contrast, east of the AAD, the crustal thickness is greater than ~7–7.5 km [*Tolstoy et al.*, 2002]. West of the AAD, the crustal structure changes significantly and the total

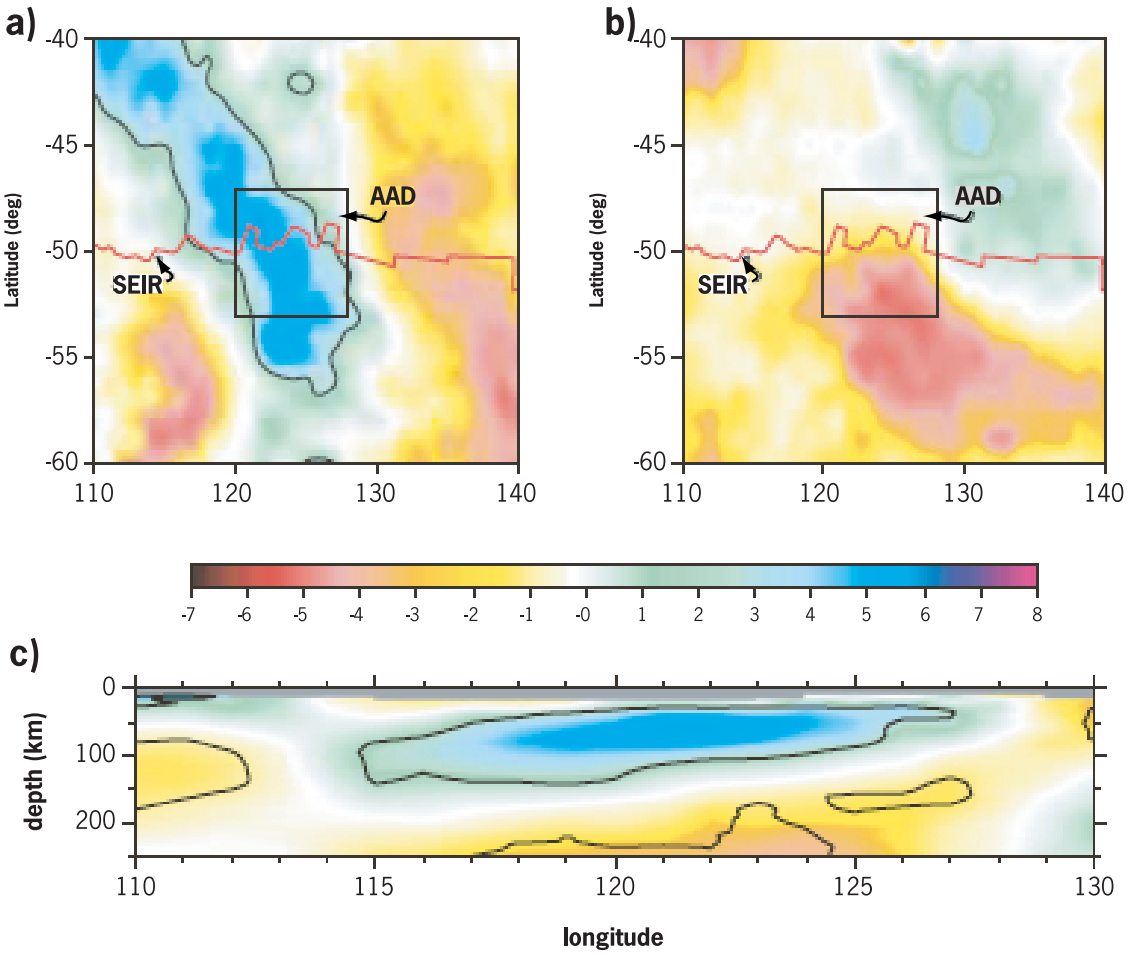

Figure 3. Images of the Australian-Antarctic Mantle Anomaly (AAMA). (a) Horizontal slice of the Vs model at 60 km depth plotted with respect to an age-dependent model. Black contours indicate +3% perturbations. (b) Similar to Figure 3a, but at 200 km depth. (c) Along-strike vertical slice. After *Ritzwoller et al.* [2003].

thickness increases from 4.2 km near 118°E to 7.2 km near 101°E [*Holmes et al.*, 2005].

[9] *Shah and Sempére* [1998] have reviewed five models relating crustal thickness and mantle temperature: two melting models [*McKenzie*, 1984; *Klein and Langmuir*, 1987] and three models based on fluid flow dynamics [*Su et al.*, 1994; *West et al.*, 1994; *Chen*, 1996]. In the present paper, we only examine the results from the melting models, which use the temperature of the melting column at the ridge axis and the temperature at the base of the lithosphere, consistent with what is used in the simple model of plate creation [*McKenzie*, 1967], which successfully accounts for the variation of depth and oceanic heat flow with age [*Parsons and Sclater*, 1977].

[10] *McKenzie* [1984] proposed a detailed model to compute the crustal thickness (e.g., the total amount of melt) generated by the isentropic upwelling of a mantle column. The model calculations depend on the entropy difference ΔS between solid and liquid per unit mass and on the variation of melt fraction by weight, X, with Pressure p and temperature T. For instance, for ΔS = 362 J kg^{-1} K^{-1}, the temperature increase (at the depth where melting begins) required for 1 km change in crustal thickness is 20°C when the T, P (in GPa) and X are linked by the following relationship: T = 1100°C + 100P + 600X. When the heat transport by melt and the gravitational energy are taken into account, the temperature increase is equal to 14°C per additional km of crust. Recently, [*McKenzie et al.*, 2005] ascribe an increase of potential temperature of 12.5°C to each km increase in crustal thickness. The potential temperature is defined to be the temperature that an element of fluid would have if it were moved adiabatically from a reference depth z_0 to a given depth z. If the mantle is in adiabatic equilibrium everywhere and if the reference depth is the Earth's surface ($z_0 = 0$), then the relation between the actual temperature T at depth z and the potential temperature T_p is

$$T_p = T \exp\left(-\frac{g\alpha z}{C_p}\right) \quad (1)$$

where α is the thermal expansion coefficient (for solid and magma, notations α_s and α_f are, respectively, used) and C_p is the specific heat at constant pressure. With $\alpha = 3 \times 10^{-5}$ K^{-1} and $C_p = 10^3$ J kg^{-1} K^{-1}, the difference between potential and real temperature amounts to about 4%. The

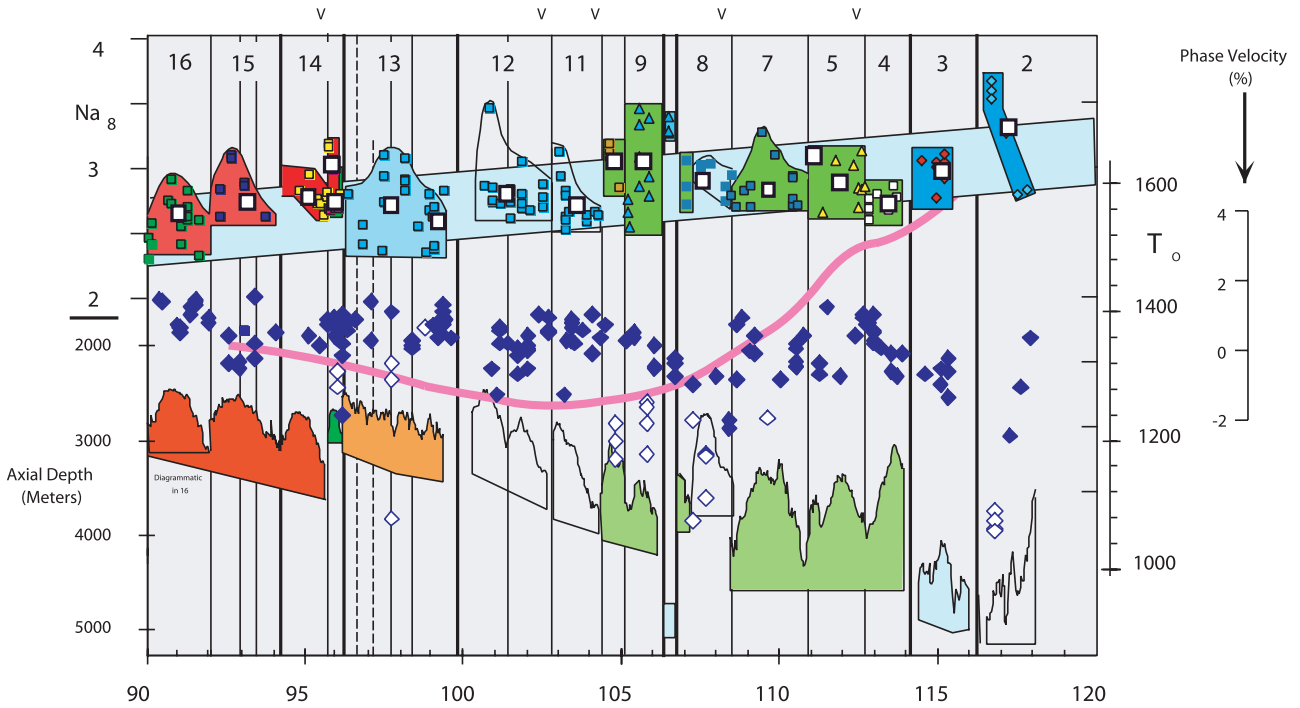

Figure 4. Profiles along the SEIR between 90°E and 118°E, showing, from top to bottom, Na_8 concentration calculated using the equation of *Klein and Langmuir* [1987]. Open squares are segment averages, smaller segments are values for individual glass groups. Smaller fields encompass the range of values for each segment. Linear background fields indicate range predicted from the global correlation of *Klein and Langmuir* [1987]. T_0 is the temperature of initial melting [*Niu and Batiza*, 1991]. Solid diamonds are normal MORBs; open diamonds are enriched MORBs. Curve behind data represents variations in Rayleigh waves phase velocity anomaly (in %) at T = 200 s [*Roult et al.*, 1994]. Axial depth is shown by the lower group of irregular fields. Shaded fields indicate intrasegment morphological transitions. Vertical lines represent segment boundaries. After *Christie et al.* [1995].

order of magnitude of the expected mantle temperature variation beneath the Southeast Indian Ridge corresponding to ~3 to 3.5 km change in crustal thickness between 88°E and 128°E could be ~50°C.

[11] This estimate is consistent with basalt geochemistry based on the analysis of major elements. [*Klein and Langmuir*, 1987] recognized a negative correlation between segment-scale averaged axial depth and Na_8 values, and between Na_8 and Fe_8 values for mid-ocean ridge basalt (MORB) glasses worldwide (Na_8 and Fe_8 are the Na_2O and FeO, respectively, content normalized at a weight percentage of MgO equal to 8%), reflecting variations in the temperature of a relatively uniform mantle. The Na_8 content of basaltic glasses from the Southeast Indian Ridge [e.g., *Christie et al.*, 1995] increases as the axial seafloor deepens between 88°E and 118° (Figure 4), in response to a decrease in the temperature of initial melting that could be of the order of ~50°C (from 1325 ± 50°C to 1375 ± 50°C), based on the work by *Klein and Langmuir* [1987].

4. Analysis of Subsidence Variations

4.1. Reassessment of Subsidence Rates

[12] The relationship between basement depth and crustal age provides a theoretically straightforward way to assess variations in mantle temperature below mid-ocean ridge crests. Assuming that the physical properties of the upper mantle are constant and that the mid-ocean ridge is isostatically compensated, seafloor depth (z) theoretically increases linearly with the square root of seafloor age (t). For young lithosphere, the relationship can be written as [e.g., *Davis and Lister*, 1974]

$$z = z_0 + \frac{2\rho_m \alpha (T_m - T_0)\sqrt{\kappa/\pi}}{(\rho_m - \rho_w)}\sqrt{t} \qquad (2)$$

where z_0 is axial depth, κ and α are the mantle thermal diffusivity and expansion coefficient, ρ_m and ρ_w are the densities of mantle and water, respectively, T_0 is the surface temperature, and T_m is the temperature of the mantle column below the rise crest. This expression, analytically derived from the half-space model, also is a good approximation for the plate model [e.g., *McKenzie*, 1967; *Parsons and Sclater*, 1977] for ages younger than ~40–50 Ma, when the temperature at the base of the plate is ascribed to be equal to T_m.

[13] Previous studies have shown that the flanks of the SEIR are characterized by lower than normal subsidence rates [e.g., *Cochran*, 1986; *Kane and Hayes*, 1994; *Sykes*, 1995]. Here, we reassess subsidence rates during the 0–25 Ma period (since the onset of the AAD-related fracture zones), using data sets that were not available prior to 1994. For bathymetry, we use the global model (topo_8.2.img) of

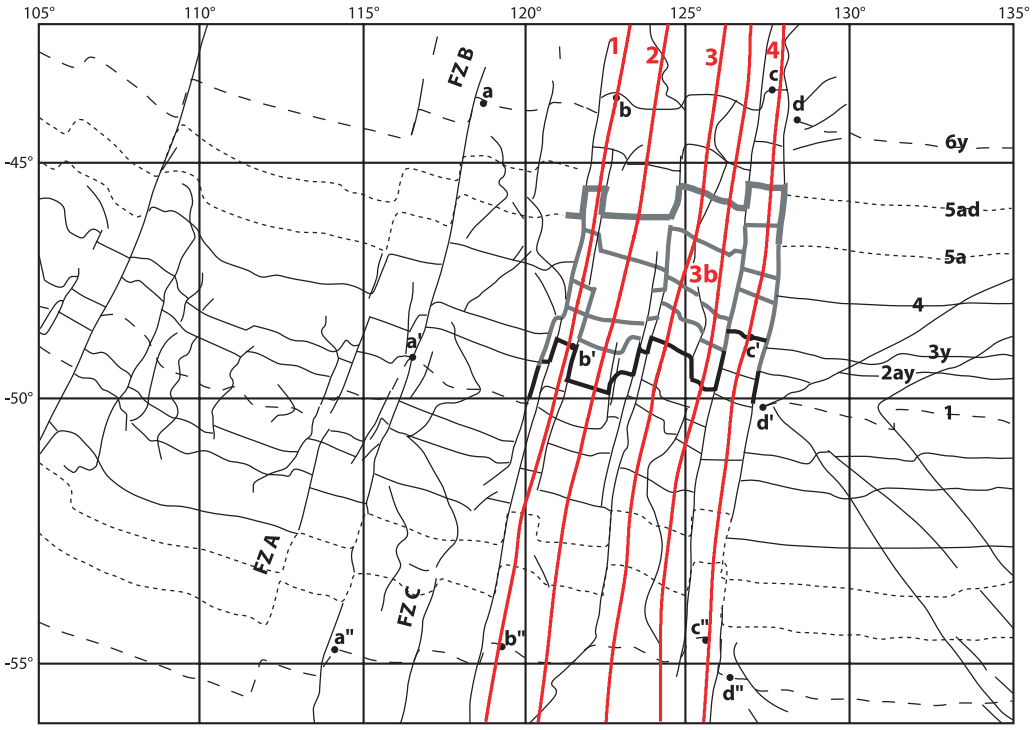

Figure 5. Isochrones based on the magnetic anomaly identification performed on the aeromagnetic data set [*Morgan et al.*, 1979; *Vogt et al.*, 1983]. Flow lines used to compute subsidence rates within the AAD are indicated by red lines. Figure caption by *Marks et al.* [1999, p. 4975] is reproduced here: "Points a', b', c', and d' along the present plate boundary were used to evaluate the degree of asymmetric spreading in various segments of the ridge system. Their conjugate points a–d lie on the 6y isochron on the Australia plate; their conjugate points a–d" are on the 6y isochron on the Antarctica plate. The distance a–a' and a'–a" are about the same (5.78, 5.88), suggesting that the spreading in the segment just east of fracture zone (FZ) B has been symmetric since Chron 6y. By contrast, distances b–b' (5.58) and c–c' (5.48) on the Australia plate are consistently shorter than the counterpart distances on the Antarctica plate (5.′8). Distance d–d' is 6.18, longer than the counterpart distance d'–d" of 5.18 on the Antarctica side." After *Marks et al.* [1999].

Smith and Sandwell [1997], based on satellite altimetry derived gravity and ship soundings. Bathymetry is inferred from gravity using a transfer function that accounts for the effect of seafloor and Moho topography. The latter effect is computed using an average crustal thickness of ~7 km and multiplied by a band pass filter that is the same everywhere. However, because the bathymetric prediction relies on gravity only at wavelengths shorter than 160 km, the fitted subsidence rate should have no influence of altimetry (W. H. F. Smith, personal communication, 2007). A deterministic approach was then followed, by carefully selecting, between 90°E and 140°E, a set of flow lines apparently unaffected by structural features, such as fracture zones, off-axis seamounts, intraplate volcanism, propagator trails, etc (Figures 1 and 2).

[14] For ages, the plate kinematics parameters of *Royer and Sandwell* [1989] were used to compute flow lines, except between 120°E and 128°E, because it does not reflect the complexity of the AAD. Within the AAD (Figure 4) we have used the age determination of *Marks et al.* [1999], who carefully identified a series of magnetic anomaly picks from closely spaced aeromagnetic profiles [e.g., *Morgan et al.*, 1979; *Vogt et al.*, 1983]. (Figure 5)

[15] In order to correct ridge flank depths for sediment thickness, we have systematically reanalyzed all available seismic reflection lines (Figure 6). These data were primarily collected during the mid 1960s and early 1970s, mainly with R/V *Eltanin*, R/V *Vema*, and R/V *Conrad*. We digitized sediment thickness along ship tracks, converted the measurements from time to depth and applied loading corrections to account for the isostatic effects of the sediments [*Crough*, 1983]. A new, regional map of sediment thickness was produced (Figure 7), which differs only slightly from the previous map of *Hayes* [1991]. Drill hole data from ODP Leg 187 [*Christie et al.*, 2004] indicate the presence of sediments 150 to 200 m thick, which suggests that the sediment cover within the AAD is unresolved by the seismic data, due to the diffraction of seismic waves on the rough seafloor topography (Table 1). The underestimation of the sediment thickness may result in errors in estimating the basement depth and subsequent underestimation of subsidence rates. Although we cannot totally preclude this hypothesis, we think that errors in sediment thickness do not change the major characteristics of the sediment pattern.

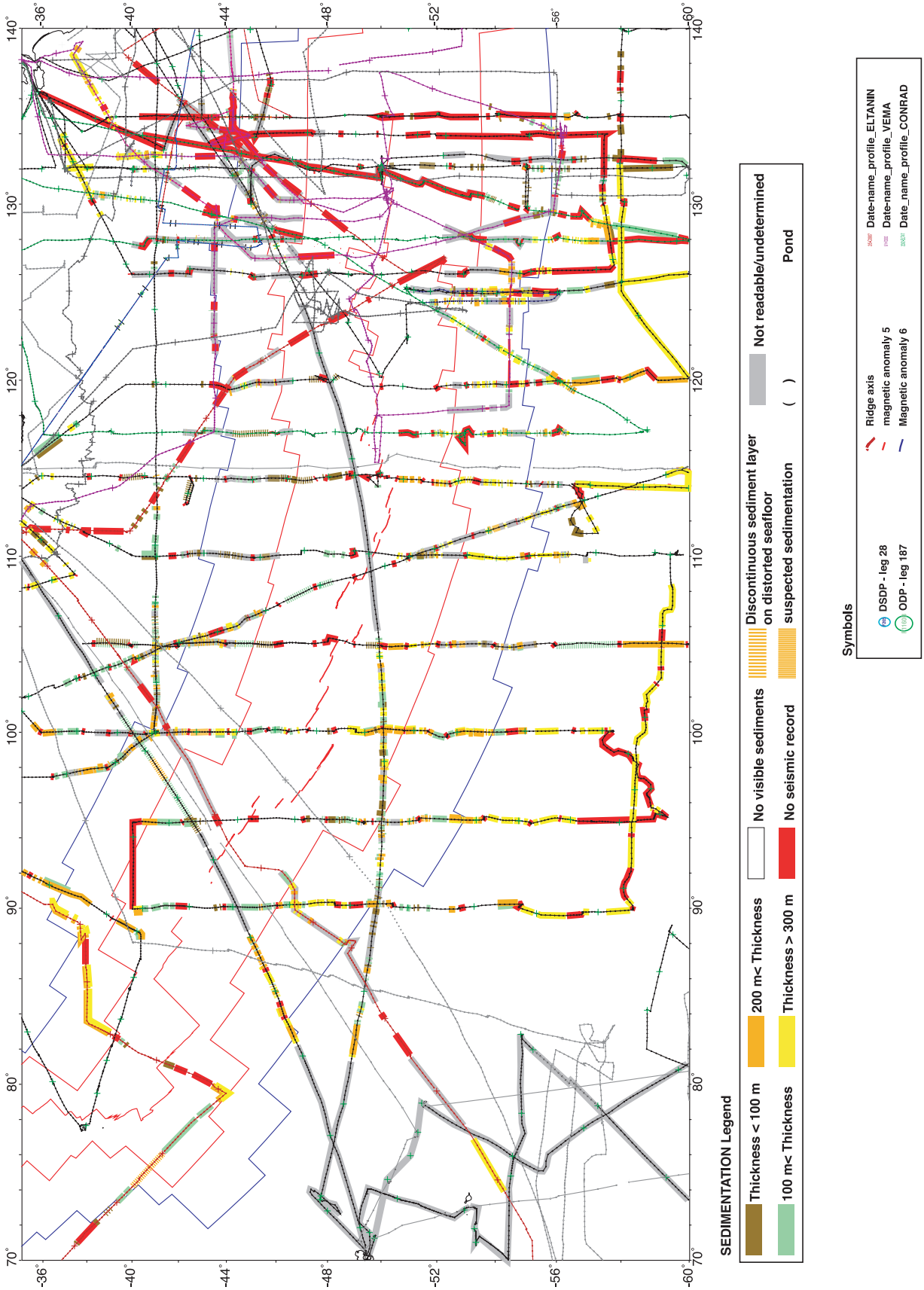

Figure 6. Available seismic lines used in the present study. Colors over track lines represent sediment thickness.

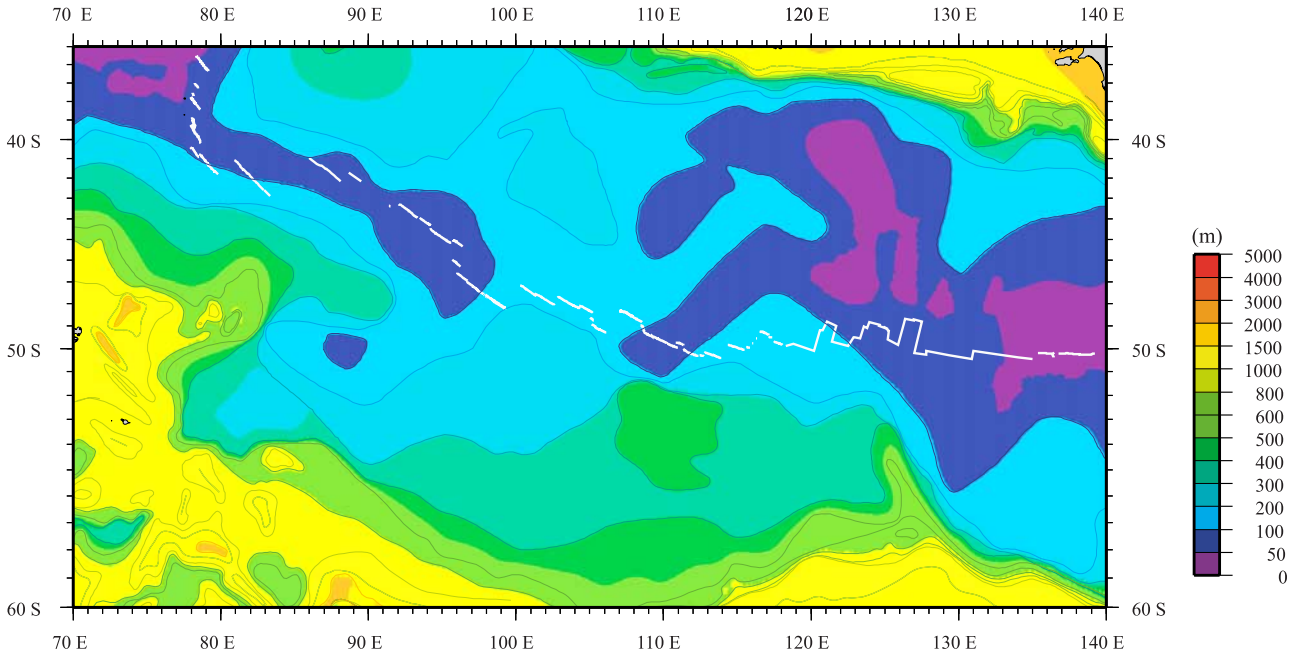

Figure 7. Revisited map of sediment thickness (in seconds two-way traveltime) with hand-contoured isopachs based on seismic lines displayed in Figure 6. Within the AAD, the sediment cover is unresolved by the seismic data. Between 90°E and 105°E, the sediment thickness resolved by the seismics is ~200–300 m on crust younger than 15 Ma but tends to increase from east to west, except in some specific, unsedimented areas.

[16] Plots of corrected basement depth versus age$^{1/2}$ along these flow lines are shown in Figure 8 (anomalous flow line 1 within the AAD, Figure 8b, has not been used to compute the averages below). Subsidence rates (Figure 9) are somewhat variable from one flow line to the next and are generally lower on crust younger than ~3–10 Ma than on older crust.

[17] On the northern flank, subsidence rates for the 0–25 Ma period are equal to 373 ± 28 (RMS) m Ma$^{-1/2}$ between longitudes 90 and 101°E; 295 ± 25 (RMS) m Ma$^{-1/2}$ between 101 and 120°E; 257 ± 13 (RMS) m Ma$^{-1/2}$ between 120 and 128°E; and 437 ± 15 (RMS) m Ma$^{-1/2}$ between 128°E and 140°E.

[18] On the southern flank, we obtain for the same age range [0–25 Ma]: 358 ± 37 (RMS) m Ma$^{-1/2}$ between longitudes 90 and 101°E; 262 ± 28 (RMS) m Ma$^{-1/2}$ between 101 and 120°E; 254 ± 10 (RMS) m Ma$^{-1/2}$ between 120 and 128°E; and 361 ± 33 (RMS) m Ma$^{-1/2}$ between 128 and 140°E.

[19] West of 101°E, subsidence rates are close to the average documented for the world's ocean basins [e.g., *Parsons and Sclater*, 1977]. We will thus hereafter use these values as reference for "normal" subsidence: 373 and 358 m Ma$^{-1/2}$ for the northern and southern flank, respectively.

[20] Subsidence values found by *Kane and Hayes* [1994] are possibly affected by uncontrolled errors due to structural effects such as ridge jumps, propagating rifts, etc. However, besides some differences, the general characteristics of the subsidence pattern are the same as those found by *Kane and Hayes* [1994] and *Hayes and Kane* [1994], except within the AAD. The gross trend is that the average subsidence rate is lower between 101°E and 120°E by about ~70–80 m Ma$^{-1/2}$. However, within the AAD, our results differ significantly from those of *Kane and Hayes* [1994]: We find that the subsidence rate is consistently lower between 120°E and 128°E than between 101°E and 128°E, whereas there is no such trend in the work by *Kane and Hayes* [1994], who used crustal ages based on the magnetic lineations of *Cande et al.* [1989], which do not reflect the complexity of the tectonic history within the AAD during the Miocene [*Marks et al.*, 1999].

[21] To summarize, our results indicate one, large-scale regional domain that extends from 101°E and 128°E, with subsidence rate less than 300 m Ma$^{-1/2}$, and one subdomain, with subsidence rate less than 260 m Ma$^{-1/2}$, delineated by

Table 1. Sediment Thickness Directly Measured at OPD Leg 187 Drill Sites[a]

Hole	Latitude	Longitude	Depth, m	Age	Sediment Thickness
1152A	41°53.9′S	127°0.4′E	5066	25.5	22
1153A	41°16.3′S	129°48.9′E	5592	28	267
1154A	41°28.7′S	131°19.0′E	5747	28	233
1155A	41°57.5′S	127°59.7′E	4986	25	177
1156A	42°44.0′S	127°53.3′E	4878	23	118
1157A	43°15.7′S	128°53.2′E	5080	22	200
1158A	43°56.9′S	128°49.7′E	5167	21	198
1159A	45°57.4′S	129°60.0′E	4515	14	145
1160A	44°0.6′S	134°59.9′E	4636	22	166
1161A	44°17.2′S	129°3.1′E	5031	19	116
1162A	44°38.0′S	129°11.3′E	5475	18	333
1163A	44°25.5′S	126°54.5′E	4365	17	160
1164A	43°44.9′S	127°44.9′E	4809	19	138

[a]From *Christie et al.* [2004]. Details are available at http://www-odp.tamu.edu/publications/prelim/187_prel/187toc.html.

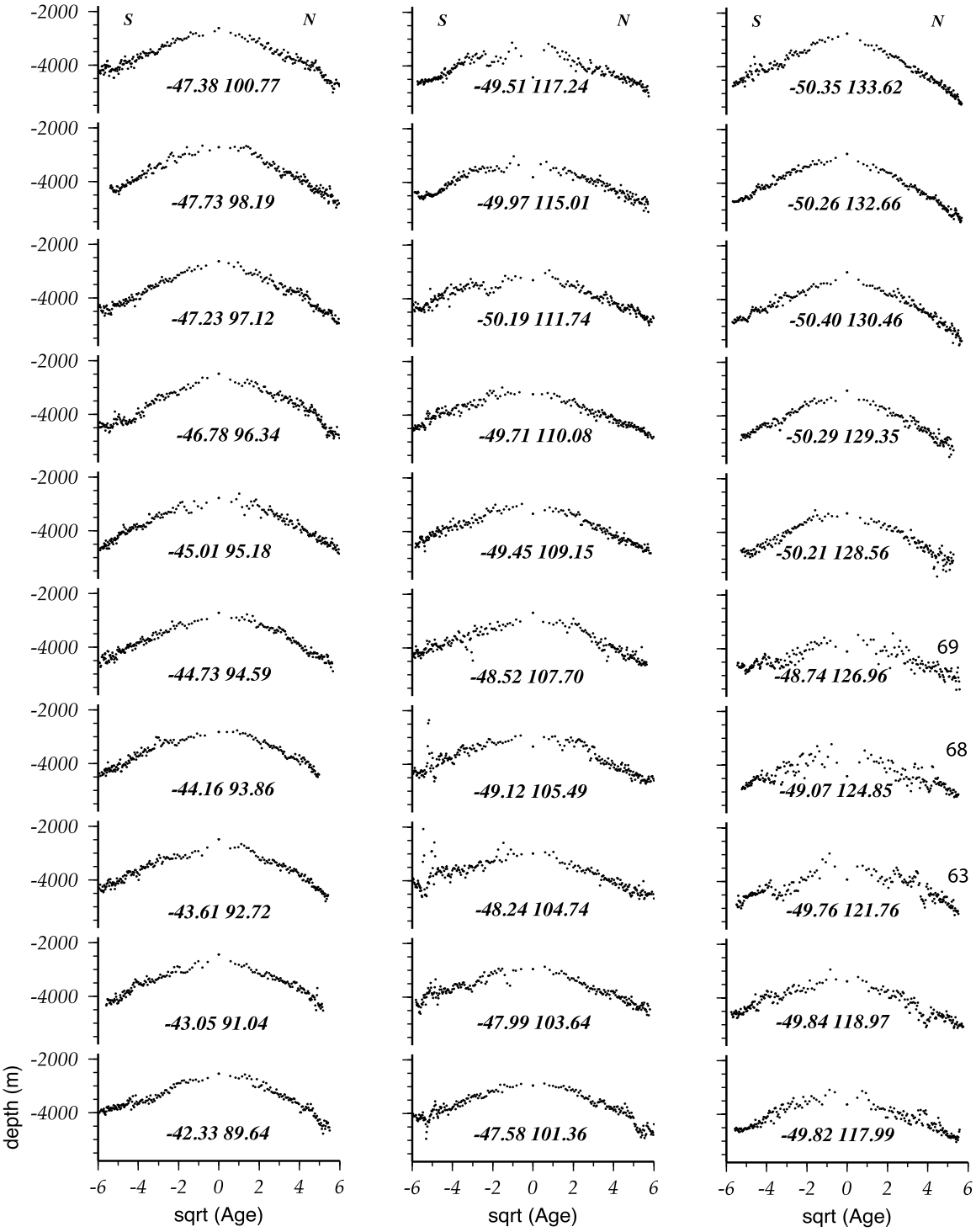

Figure 8a. Basement depth plotted versus the square root of crustal age along selected flow lines crossing the SEIR between 90°E and 133.6°E. Flow lines are based on the plate kinematics parameters of *Royer and Sandwell* [1989]. Zero-age coordinates are indicated for every flow line. Note the very low subsidence rates between 0 and ~5–9 Ma as well as the slightly arcuate shape of the curves, which indicates that the subsidence rate progressively increases with age in the 0–25 Ma period.

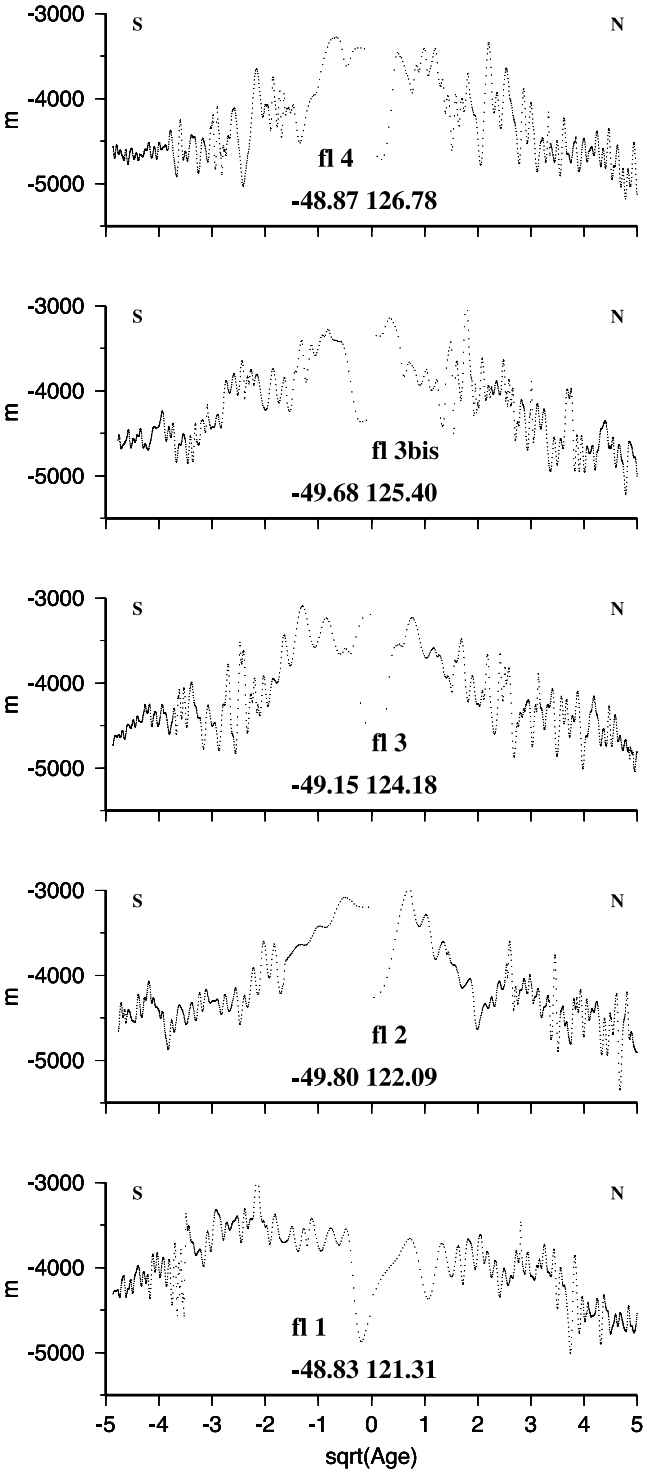

Figure 8b. Basement depth plotted versus the square root of crustal age along selected flow lines crossing the SEIR between 120°E and 128°E (see location in Figure 2) based on the kinematic parameters (poles and rotation angles) of *Marks et al.* [1999]. Zero-age coordinate is indicated for every flow line. Flow line numbers refer to those indicated in Figures 2 and 5. Note that the subsidence averages (see text) between 120°E and 128°E have been computed without flow line 1.

two prominent fracture zones: near 120°E and 128°E, respectively. The change in subsidence rate is very abrupt across both fracture zones.

4.2. Temperature Dependence of the Mantle Physical Properties

[22] Using commonly accepted, constant thermal parameters ($\alpha = 3 \times 10^{-5}\,K^{-1}$, $\kappa = 10^{-6}\,m^2\,s^{-1}$; $\rho_m = 3300\,kg\,m^{-3}$) [*Lister*, 1977] and equation (1), temperature variations of about 350°C would be required to explain variations in thermal subsidence of 100 m $Ma^{-1/2}$, which is unrealistic. Low values of α and κ between 101°E and 128°E may partially explain part of the observed low subsidence rates. This ad hoc explanation is possible, but not satisfying because it cannot be supported by direct estimates of the mantle thermal parameters, while indirect estimates are affected by very large uncertainties [*Patriat and Doucouré*, 1992].

[23] The temperature dependence of the mantle physical properties (k, α, ρ, C_p) and the variable initial temperature of the melting column beneath the ridge axis do affect the subsidence rate [*McKenzie et al.*, 2005]. We follow the approach of *McKenzie et al.* [2005] to analytically compute an overestimate of the subsidence rate variation that would result in response to a temperature change at the base of the plate. If active heat generation within the lithosphere and horizontal heat conduction are ignored, the temperature T(z, t) within a cooling plate satisfies

$$\frac{\partial[\rho(T)C_p(T)T]}{\partial t} = \frac{\partial}{\partial z}\left[k(T)\frac{\partial T}{\partial z}\right] \tag{3}$$

[24] The equation being nonlinear, *McKenzie et al.* [2005] introduce the integral

$$G = \int k(T)dT \tag{4}$$

and write equation (3) as

$$\frac{\partial T}{\partial t} = \frac{1}{\rho C_p}\frac{\partial^2 G}{\partial z^2} - \frac{T}{\rho C_p}\frac{\partial(\rho C_p)}{\partial t} \tag{5}$$

[25] The second term on the right-hand side being considerably smaller than the first, it is hereafter ignored. *McKenzie et al.* [2005] derive the temperature field by solving the resulting equation using standard methods. Then, they approximate the subsidence s(t) below the depth of the ridge by assuming isostatic compensation:

$$s(t) = \frac{1}{(\rho_m^0 - \rho_w)}\left\{\int_0^L \rho[T(0,z)]dz - \int_0^L \rho[T(t,z)]dz\right\} \tag{6}$$

[26] The expression proposed is accurate to O(αT). The subsidence rate per square root of age is

$$a(t) = \frac{\partial s(t)}{\partial(\sqrt{t})} = 2\sqrt{t}\frac{\partial s(t)}{\partial(t)} = -2\sqrt{t}\frac{1}{(\rho_m^0 - \rho_w)}\int_0^L \frac{\partial T(t,z)}{\partial t}\frac{\partial \rho(T)}{\partial T}dz \tag{7}$$

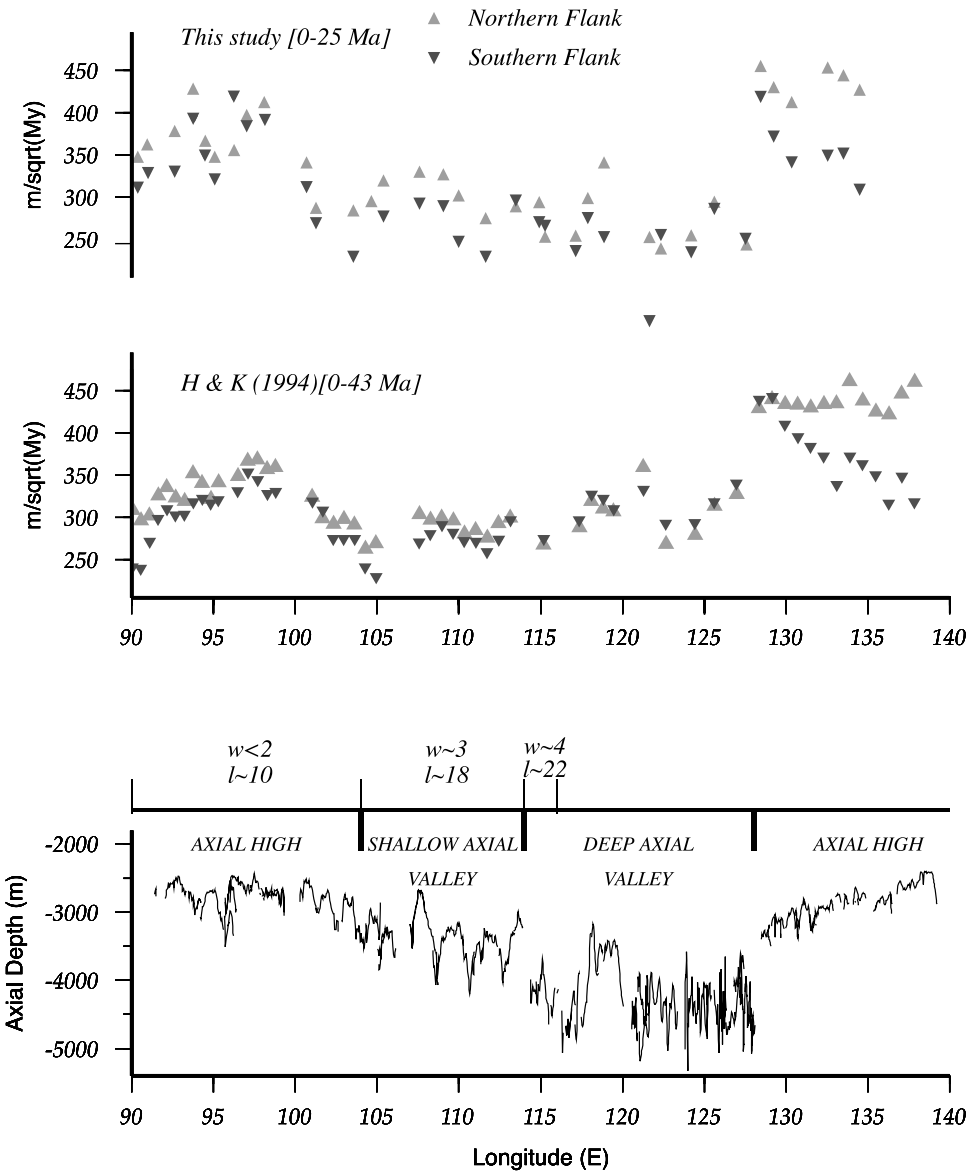

Figure 9. (bottom) Bathymetric profile (plotted versus longitude) along the axis of the South Indian Ridge. Indications on axial morphology are after *Cochran et al.* [1997]. Average characteristic width (w) and length (l) of abyssal hills are in km, based on work by *Goff et al.* [1997]. (top) Along-axis subsidence rates variations plotted versus longitude. (middle) The [0–42 Ma] age range [after *Hayes and Kane*, 1994]. (top) This study subsidence rates, reassessed for the 0–25 Ma age range. Triangles and inverted triangles are for the northern and southern flanks, respectively.

[27] Then, ignoring the second term on the right-hand side of equation (5), we obtain

$$a(t) = -2\sqrt{t}\frac{1}{\left(\rho_m^0 - \rho_w\right)}\int_0^L \frac{1}{\rho C_p}\frac{\partial^2 G}{\partial^2 z}\left[\frac{\partial \rho(T)}{\partial T}\right]_P dz \qquad (8)$$

[28] Using the same relation between α(T) and ρ(T) as *McKenzie et al.* [2005], we derive

$$a(t) = 2\sqrt{t}\frac{1}{\left(\rho_m^0 - \rho_w\right)}\int_0^L \frac{\alpha(T)}{C_p(T)}\frac{\partial^2 G}{\partial^2 z}dz \qquad (9)$$

[29] From the definition of G (equation (4)), we get

$$a(t) = 2\sqrt{t}\frac{1}{\left(\rho_m^0 - \rho_w\right)}\int_0^{T_m} \frac{\alpha(T)}{C_p(T)}\frac{\partial\left[k(T)\dfrac{\partial T}{\partial z}\right]}{\partial T}dT \qquad (10)$$

where T_m is the mantle temperature at the base of the plate. Let us now evaluate the difference in subsidence rate for two different thermal configurations within the mantle, A and B, characterized by different plate thicknesses and basal temperatures: L_A, T_m^A and L_B, T_m^B, respectively, with $T_m^B > T_m^A$ (as pointed out by *McKenzie et al.* [2005], the crustal thickness fixes the potential temperature of the mantle; hence only the thickness of the lithosphere remains as an adjustable parameter to fit the depth and heat flow

Table 2. Temperature Dependence of α(T), k(T), ρ(T) and C_P(T) Used by *McKenzie et al.* [2005][a]

Physical Properties	Dependence on Temperature	Coefficients
Thermal expansion coefficient	$\alpha(T) = \alpha_0 + \alpha_1 T$	$\alpha_0 = 2.832 \times 10^{-5}$ K^{-1} $\alpha_1 = 3.79 \times 10^{-8}$ K^{-2}
Thermal conductivity	$k(T) = \frac{b}{1+c(T-273)} + d_0 + d_1 T + d_2 T^2 + d_3 T^3$	b = 5.3 W m^{-1} K^{-1} c = 0.0015 K^{-1} $d_0 = 1.753 \times 10^{-2}$ W m^{-1} K^{-1} $d_1 = -1.0365 \times 10^{-4}$ W m^{-1} K^{-2} $d_2 = 2.2451 \times 10^{-7}$ W m^{-1} K^{-3} $d_3 = -3.4071 \times 10^{-11}$ W m^{-1} K^{-4}
Density	$\rho(T) = \rho_0 + \exp(-[\alpha_0(T - T_0) + \frac{\alpha_1}{2}(T^2 - T_0^2)]$	$\rho_0 = 3330$ kg m^{-3} $T_0 = 273$ K
Specific heat at constant pressure	$C_P(T) = k_0 + \frac{k_1}{\sqrt{T}} + \frac{k_3}{T^3}$	$k_0 = 1.65 \times 10^3$ J kg^{-1} K^{-1} $k_1 = -12.80 \times 10^3$ J kg^{-1} K$^{-1/2}$ $k_3 = -0.19 \times 10^{10}$ J kg^{-1} K^{-2}

[a] T is expressed in K. For specific heat, experimental values for forsterite are used. To convert J mol^{-1} into J kg^{-1}, the molecular weight of forsterite was taken equal to 140.69.

observations wherever the crustal thickness is known; where it is not known, both L and T_m are required). Let $T_A(z, t)$ and $T_B(z, t)$ be the respective temperature fields within the plate, solutions of equation (5); $a_A(t)$ and $a_B(t)$ are the corresponding subsidence rate. We write

$$a_B(t) - a_A(t) = 2\sqrt{t}\frac{1}{(\rho_m^0 - \rho_w)} \cdot \left\{ \int_0^{T_m^A} \frac{\alpha(T)}{C_p(T)} \frac{\partial\left(k(T)\frac{\partial(T_B - T_A)}{\partial z}\right)}{\partial T} dT + \int_{T_m^A}^{T_m^B} \frac{\alpha(T)}{C_p(T)} \frac{\partial\left(k(T)\frac{\partial T_B}{\partial z}\right)}{\partial T} dT \right\} \quad (11)$$

[30] The second term of the sum of the right-hand side in equation (11) is much smaller than the first and consequently, it is ignored. The derivative with respect to T in the integral of the first term of the sum has a constant, negative sign between 0 and T_m^A. Hence the difference in subsidence rate between configurations A and B can be approximately overestimated as follows:

$$|a_B(t) - a_A(t)| \le 2\sqrt{t}\frac{1}{(\rho_m^0 - \rho_w)} \cdot \underbrace{\max\left[\frac{\alpha(T)}{C_p(T)}\right]}_{[0,T_A]} \left[k(T)\frac{\partial(T_A - T_B)}{\partial z}\right]_0^{T_m^A} \quad (12)$$

[31] Because the term in the square bracket is a difference, it can be approximated (to the first order) using the analytical solution, $T_A^{PM}(z,t)$, proposed by *Parsons and Sclater* [1977] for a plate of thickness L_A at temperature T_m^A (for configuration B, exchange subscripts, from A to B). We thus obtain the following approximation:

$$|a_B(t) - a_A(t)| \le 2\sqrt{t}\frac{1}{(\rho_m^0 - \rho_w)} \cdot \underbrace{\max\left[\frac{\alpha(T)}{C_p(T)}\right]}_{[0,T_A]} \left[k(T)\frac{\partial(T_A^{PM} - T_B^{PM})}{\partial z}\right]_0^{T_m^A} \quad (13)$$

[32] At great depths, the thermal gradient decreases to zero, so that the term in brackets can be approximated. We get

$$|a_B(t) - a_A(t)| \le 2\sqrt{t}\frac{1}{(\rho_m^0 - \rho_w)} \underbrace{\max\left[\frac{\alpha(T)}{C_p(T)}\right]}_{[0,T_A]} |q_B^{PM} - q_A^{PM}| \quad (14a)$$

where q_A^{PM} stands for the theoretical surface heat flow based on the *Parsons and Sclater* [1977] model. For ages younger than about ~40–50 Ma, the analytical expression for temperature based on the half-space model approximation [e.g., *Davis and Lister*, 1974] can be used to obtain

$$|a_B(t) - a_A(t)| \le 2\sqrt{t}\frac{\rho_m^0 \alpha(0)}{(\rho_m^0 - \rho_w)} \cdot \sqrt{\frac{\kappa(0)}{\pi}} |T_m^B - T_m^A| \frac{\alpha(T_m^A)}{\alpha(0)} \frac{C_P(0)}{C_P(T_m^A)} \quad (14b)$$

[33] Using $T_m^A = 1300$°C and the numerical values (Table 2) based on the work by *McKenzie et al.* [2005], we obtain that a change in mantle temperature of ~50°C at the base of the plate cannot produce a change in subsidence rate any greater than about 35 m Ma$^{-1/2}$. Hence the observed variations in subsidence rate along the SEIR for the 0–25 Ma period cannot be explained solely by changes in mantle temperature (Table 2).

4.3. Crustal Thickness Variations

[34] Crustal thickness variations can dramatically affect residual depth anomalies [*Marks et al.*, 1990], but not necessarily subsidence rates. Abrupt crustal thinning at a given age theoretically affects seafloor deepening by producing a characteristic saw tooth in the depth–age$^{1/2}$ profile, and by slightly affecting the slope of the curve in response to the mantle temperature variation that produced the crustal thinning. Basalts geochemistry consistently indicates that Indian mantle lavas have been derived by smaller degrees of melting than Pacific mantle lavas throughout the last ~28 Ma [*Christie et al.*, 2004]. Hence the spatially abrupt change of subsidence rate across the eastern bound-

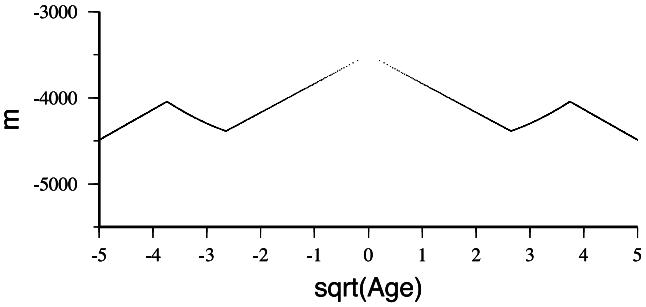

Figure 10. Seafloor depth versus square root of age (Ma), computed with a plate model, assuming that the mantle temperature progressively decreased between 14 and 7 Ma, from 1300°C to ~1230°C. The resulting theoretical subsidence curve does not reflect the shape of the observed curves (Figure 8).

ary of the AAD is not due to the difference in crustal thickness from one region to the other.

[35] Within the AAD, the Indian mantle-derived basalts that were collected during ODP Leg 187 (on crust aged between 14 and 28 Ma) differ from those dredged near the spreading axis (0–7 Ma), indicating that the melt production decreased between 14 and 7 Ma [*Christie et al.*, 2004; M. Russo et al., manuscript in preparation, 2007]. Because there are no samples from 7 to 14 Ma seafloor, it is unclear whether this decrease was gradual or incremental. Let us thus assume that mantle temperature progressively decreased between 14 and 7 Ma, from 1300°C to ~1230°C (corresponding to an extreme change in crustal thickness from 7 to 3 km). The resulting theoretical subsidence curve (Figure 10) does not reflect the shape of the observed curves (Figure 8). This result and the absence of discernible temporal or spatial gradients in either the 14 to 28 Ma Leg 187 data set or the 0 to 7 Ma near-axis data set suggest that the decrease in mantle temperature was most likely abrupt and related to either or both of two significant tectonic events documented in tectonic reconstructions by *Marks et al.* [1999]. For all practical purposes, we hence conclude that a major change in crustal thickness occurred before 25 Ma, at the onset of the large fracture zones. The other changes that may have occurred within the AAD during the last 25 Ma were more subtle, with little effect on the subsidence curves.

4.4. Dynamic Effects

[36] Since the early 1970s, the AAD has been proposed to be the locus of deep seated dynamic effects [e.g., *Weissel and Hayes*, 1974]. If such effects are present, the SEIR topography is not compensated beneath the AAD and the half-space or the plate cooling models do not apply (equation (2) does not hold). The major problem is that the quantitative assessment of dynamic topography greatly depends on the physical model that is used to explain its existence. Because the Australian-Antarctic Depth Anomaly across the ocean basin reflects a cold anomaly within the mantle that persisted since at least ~100 Ma, our preferred hypothesis is that of *Gurnis et al.* [2002], according which the AAD could be located above a remnant, fossil slab that subducted to the southwest below the Australian Continent (Figure 11a), which was then part of Gondwanaland, during upper Cretaceous times [*Gurnis et al.*, 1998, 2000]. Recently, *Gurnis and Müller* [2003] proposed model including a mantle wedge above the subducting slab that they state is consistent with (1) thinner crust and chaotic seafloor topography suggesting that a cold spot is presently being sampled within the AAD; (2) the continuous sampling by the SEIR of a cold anomaly since at least 45 Ma followed by a pulse resulting in the abrupt onset of fracture zone at ~20 to 25 Ma; and (3) the existence of a high-velocity (presumably cold) trapped transition zone anomaly.

[37] On the basis of the work by *Gurnis and Müller* [2003], the computed contribution to the observed seafloor topography (Figure 11), however, appears to be significant only within the AAD; west of 115°E, it dramatically decreases to zero. Therefore, while AAD-related dynamic effects may partially contribute to anomalous seafloor deepening between 120°E and 128°E, they cannot explain the subsidence pattern to the west of the AAD, e.g., between 101°E and 115°E, nor the abruptness of the subsidence rate variation across the eastern boundary of the AAD.

4.5. Effect of "Ubiquitously Distributed" Melt Within the Asthenosphere

[38] Partial melt is generally accepted to be a primary factor that influences mantle shear wave velocity anomalies (see for instance the recent, detailed discussion of *Priestley and McKenzie* [2006]. *Forsyth* [1992, p. 29] noted that "a velocity anomaly of 0.35 km/s (derived from observed travel time differences) in the 20-40 km depth range below the AAD would require an unrealistic mantle temperature difference. . .without the involvement of melt. In contrast, it could be explained by a change in melt fraction. . .requiring a temperature change of less than 100°C." Following *Turcotte and Schubert* [1982, p. 183], let us hence assume that (1) the lithosphere thickness $y_L(t)$ at a given age t corresponds to the depth at which the mantle is entirely solid and (2) the asthenospheric mantle, below $y_L(t)$, contains an homogeneous melt fraction, hereafter noted φ_m, a regionally averaged melt fraction in volume (Figure 12). Then the density of lithosphere (ρ_L) and wet asthenosphere (ρ_m^a) are

$$\rho_m^a \approx \rho_m\left[1-\varphi_m\right]+\rho_m^f\varphi_m \tag{15a}$$

$$\rho_L(T) \approx \rho_m[1-\alpha(T-T_m)] \tag{15b}$$

respectively, where ρ_m and ρ_m^f, stand for the solid and liquid mantle densities (the expansion coefficient α is for solid mantle). For young ages (<40 to 50 Ma), the temperature field within the boundary layer is again expressed using the half-space model approximation. Assuming isostatic compensation at the base of the plate, seafloor depth

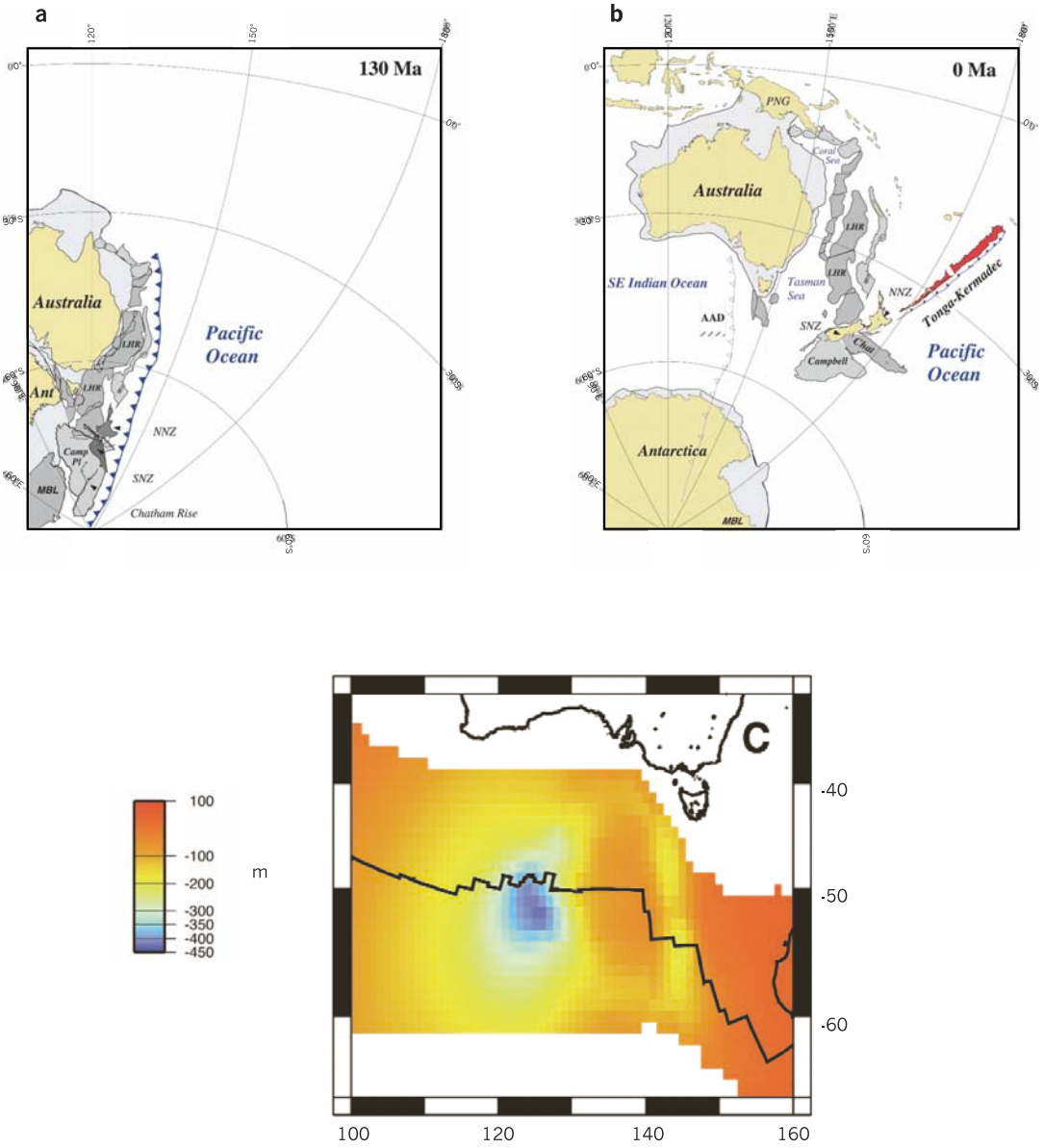

Figure 11. Plate tectonics reconstructions indicate the position of the subduction zone bordering Eastern Gondwana (a) 130 Ma ago and (b) the present-day position of a hypothesized detached slab below the AAD. (c) Computed dynamic seafloor topography resulting from the detached slab. Image is based on elements provided by M. Gurnis and D. Müller (for details, see *Gurnis and Müller* [2003]).

can be written as follows [*Turcotte and Schubert*, 1982, Pioneer 183]:

$$z = z_0 + \frac{\rho_m \alpha (T_m - T_0)}{(\rho_m - \rho_v)\left(1 - \varphi_m \dfrac{\rho_m - \rho_l}{\rho_m - \rho_w}\right)} \cdot 2\sqrt{\frac{\kappa t}{\pi}} + \frac{\varphi_m (\rho_m - \rho_l)}{(\rho_m - \rho_w)\left(1 - \varphi_m \dfrac{\rho_m - \rho_l}{\rho_m - \rho_w}\right)} y_L(\mathrm{t}) \tag{16}$$

[39] Using the physics of sill solidification, *Turcotte and Schubert* [1982, pp. 172–174] derive the depth of the solidification interface, $y_L(t)$, by balancing the heat conducted away from this interface and the heat released by solidification:

$$y_L(t) = 2\lambda_1 \sqrt{\kappa t} \tag{17}$$

where λ_1 is solution of

$$\varphi_m \frac{H_L \sqrt{\pi}}{C_p T_m} = \frac{e^{-\lambda_1^2}}{\lambda_1 \mathrm{erf}(\lambda_1)} \tag{18}$$

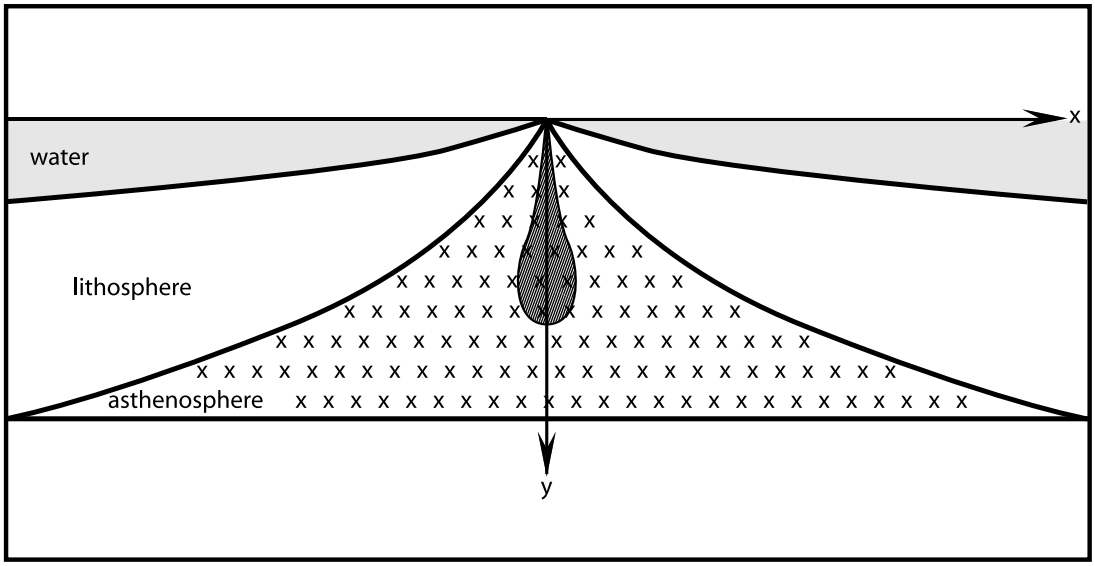

Figure 12. Sketch explaining the signification of parameter φ_m: an "homogeneous melt fraction," which would be equally distributed within the asthenosphere (crossed area). This parameter is supposed to depend on the mantle temperature, T_m, at the base of the plate. This parameter φ_m must not be mistaken with the partial melt fraction (a function of P and T) that characterizes the zone below the ridge from which melt is extracted to produce the axial crust (grey area).

and H_L and C_p are the mantle latent and specific heat, respectively. Note that in equation (17), $y_L(t)$ is proportional to the square root of age to the first order. The linear relation between seafloor depth and $\sqrt{t}$ is thus preserved in equation (16), which can be rewritten as follows:

$$z = z_0 + \left[\underbrace{\frac{\rho_m \alpha (T_m - T_0)}{(\rho_m - \rho_v)\left(1 - \varphi_m \dfrac{\rho_m - \rho_l}{\rho_m - \rho_w}\right)} 2\sqrt{\frac{\kappa}{\pi}}}_{S1} + \underbrace{\frac{\varphi_m (\rho_m - \rho_l)}{(\rho_m - \rho_w)\left(1 - \varphi_m \dfrac{\rho_m - \rho_l}{\rho_m - \rho_w}\right)} 2\lambda_l \sqrt{\kappa}}_{S2} \right] \sqrt{t} \qquad (19)$$

[40] The first term (S_1) of the right-hand side of equation (19) corresponds to the subsidence in absence of partial melt, while the second term (S_2) is the contribution of partial melt. Parameter φ_m, as defined by *Turcotte and Schubert* [1982], is a "homogeneous melt fraction," which would be equally distributed within the asthenosphere. This parameter depends on mantle temperature, T_m. Of regional significance, it is used to characterize the average density of the asthenosphere and has some bearing to seismic wave velocities. Hence it can be used to correlate seismic velocity and seafloor subsidence anomalies below ocean basins. This parameter φ_m must not be mistaken with the partial melt fraction, a function of P and T, that characterizes the zone below the ridge from which melt is extracted to produce the axial crust. Mantle density variations due to partially molten rocks within this zone have hardly any effect on seafloor depth after a few millions years.

[41] Including the effect of ubiquitously distributed partial melt, φ_m, adds term (S_2) to (S_1), the subsidence rate obtained in absence of melt. Fitting equation (19) to the data thus requires the adjustment of 4 parameters, instead of 3: α, κ, T_m, but also φ_m. The absolute value of φ_m needs to be known, while α and κ need to be readjusted (α and κ must be lower than expected when no melt is present). Such an enterprise is beyond the scope of the present paper. Absolute estimates of φ_m are not easy, if not impossible to obtain, but variations in melt fraction ($\Delta\varphi_m$) can be approximated using general relationships between seismic velocity and melt fraction within the mantle. On the basis of the work by *Ritzwoller et al.* [2003], shear wave velocity negative anomalies at 100 km depth below the AAD do not exceed 8%, which, according to model calculations can be ascribed to variations in melt fraction of 1% or less [e.g., *Hammond and Humphreys*, 2000]. For $\kappa = 10^{-6}$ m^2, $H_L = 400$ kJ kg^{-1}, $T_m =$ 1300 °C and $\Delta\varphi_m < -1\%$, we obtain $S_2 < -25$ m Ma$^{-1/2}$.

[42] Depletion of ubiquitously distributed melt within the asthenosphere is consistent with the existence of the Australian-Antarctic mantle anomaly resolved by *Ritzwoller et al.* [2003] extending to the west of the AAD. It may significantly contribute to the low subsidence rates observed within the AAD for the [0–25 Ma] period. However, it does not explain the sharpness of the subsidence rate variation across the eastern boundary of the AAD.

5. Conclusions

[43] Anomalously low subsidence rates characterize the flanks of the Southeast Indian Ridge for the 0–25 Ma period (subsidence of seafloor is less than 300 m Ma$^{-1/2}$ between 101°E and 118°E and less than 260 m Ma$^{-1/2}$

between 120°E and 128°E) while geophysical and geochemical evidence suggest that the expected along-axis variation in mantle temperature below the ridge crest probably does not exceed ~50°C. The variation of α and k with T affect the deepening of the seafloor with age, but the expected mantle temperature variations are too small to explain the full range of subsidence rate variations between 101°E and 128°E. These cannot be explained by one single effect but by a combination of factors in addition to mantle temperature.

[44] We successively considered four different factors: (1) the temperature dependence of the mantle physical properties; (2) variations in crustal thickness in response to an abrupt or progressive (between 7 and 14 Ma) mantle temperature decrease inferred from AAD basalts geochemistry; (3) dynamic effects possibly created by an old, detached slab which subducted below Eastern Gondwana, creating a cold zone within the mantle below the AAD [*Gurnis et al.*, 2000]; and (4) depletion in the "ubiquitously distributed melt fraction" (φ_m) that characterizes the asthenosphere.

[45] These effects may all contribute to the observed, anomalously low subsidence rate of the ridge flanks, with the most significant contribution being probably related to the depletion in φ_m. However, these effects have a deep-seated origin within the upper mantle, resulting in long-wavelength geophysical variations. They altogether probably explain that the subsidence is anomalously low between 101°E and 128°E. None of them can explain the abruptness of the transition across the fracture zones that delineate the boundaries of the AAD, near 120°E and near 128°E, respectively.

[46] **Acknowledgments.** This work was initiated as L.G. was a Cecil and Ida Green scholar at IGPP, Scripps Institution of Oceanography, San Diego. Discussions with numerous colleagues at IGPP were very helpful. Marc Russo (COAS, Oregon State University) provided an unpublished manuscript on the evolution of the AAD, viewed from the geochemical perspective. Walter Smith provided advice on the use of satellite-derived bathymetry for evaluating subsidence rates. The GMT software was used [*Wessel and Smith*, 1991]. Laetitia Morvan finalized the figure drawings. LDEO contribution 7047.

References

Cande, S. C., and J. Mutter (1982), A revised identification of the oldest seafloor spreading anomalies between Australia and Antarctica, *Earth Planet. Sci. Lett.*, *58*, 151–160.

Cande, S. C., J. L. Labrecque, R. L. Larson, and W. C. Pitman III (1989), Magnetic lineations of the world's ocean basins, Am. Assoc. of Pet. Geol., Tulsa, Okla.

Chen, Y. (1996), Constraints on melt production rate beneath the mid-ocean ridges based on passive fluid flow models, *Pure Appl. Geophys.*, *146*, 589–620.

Chen, Y., and J. Morgan (1990), Rift valley/no rift valley transition at mid-ocean ridges, *J. Geophys. Res.*, *95*, 17,571–17,581.

Christie, D. M., B. Sylvander, and F. Sprtel (1995), Major elements variability of basalts from the southeast Indian Ridge between 88°E and 118°E, *Eos Trans. AGU*, *76*, Fall Meet. Suppl., F529.

Christie, D., B. P. West, D. G. Pyle, and B. B. Hanan (1998), Chaotic topography, mantle flow and migration in the Australian Antarctic Discordance, *Nature*, *394*, 637–644.

Christie, D. M., D. G. Pyle, R. B. Pedersen, and D. J. Miller (2004), Leg 187 synthesis: Evolution of the Australian Antarctic Discordance, the Australian Antarctic depth anomaly, and the Indian/Pacific mantle isotopic boundary, *Proc. Ocean Drill. Program Sci. Results* [Online], *187*. (Available at http://www-odp.tamu.edu/publications/187_SR/synth/synth.htm)

Cochran, J. R. (1986), Variations in subsidence rates along intermediate and fast spreading mid-ocean ridges, *Geophys. J. R. Astron. Soc.*, *87*, 421–454.

Cochran, J. R., J. Sempéré, and SEIR Scientific Team (1997), The Southeast Indian Ridge between 88°E and 118°E: Gravity anomalies and crustal accretion at intermediate spreading rates, *J. Geophys. Res.*, *102*, 15,463–15,488.

Crough, T. (1983), The correction of sediment loading on the seafloor, *J. Geophys. Res.*, *88*, 6449–6454.

Davis, E. E., and C. R. B. Lister (1974), Fundamentals of ridge crest topography, *Earth Planet. Sci. Lett.*, *21*, 405–413.

Forsyth, D. W. (1992), Geophysical constraints on mantle flow and melt generation beneath Mid-Ocean Ridges, in *Mantle Flow and Melt Generation at Mid-ocean Ridges*, *Geophys. Monogr. Ser.*, vol. 71, edited by J. P. Morgan, pp. 1–65, AGU, Washington, D. C.

Forsyth, D., R. L. Ehrenbard, and S. Chapin (1987), Anomalous upper mantle beneath the Australian-Antarctic Discordance, *Earth Planet. Sci. Lett.*, *84*, 471–478.

Goff, J. A., Y. Ma, A. Shah, J. R. Cochran, and J. Sempéré (1997), Stochastic analysis of seafloor morphology on the flank of the Southeast Indian Ridge: The influence of ridge morphology on the formation of abyssal hills, *J. Geophys. Res.*, *102*, 15,521–15,534.

Gurnis, M., and R. D. Müller (2003), Origin of the Australian-Antarctic Discordance from an ancient slab and mantle wedge, *Spec. Publ. Geol. Soc. Aust.*, *22*, 411–423.

Gurnis, M., R. D. Müller, and L. Moresi (1998), Dynamics of Cretaceous vertical motion of Australia and the Australian-Antarctic Discordance, *Science*, *279*, 1499–1504.

Gurnis, M., M. Moresi, and R. D. Müller (2000), Models of mantle convection incorporating plate tectonics: The Australian region since the Cretaceous, in *The History and Dynamics of Global Plate* Motions, *Geophys. Monogr. Ser.*, vol. 121, edited by M. A. Richards, R. Gordon, and R. van der Hilst, pp. 211–238, AGU, Washington, D. C.

Hammond, W. C., and E. D. Humphreys (2000), Upper mantle seismic wave velocity: Effects of realistic partial melt geometries, *J. Geophys. Res.*, *105*, 10,975–10,986.

Hayes, D. E. (1991), *Marine Geological and Geophysical Atlas of the Circum-Pacific to 30°S*, *Antarct. Res. Ser.*, vol. 54, AGU, Washington, D. C.

Hayes, D. E., and J. R. Conolly (1972), Morphology of the southeast Indian Ocean, in *Antarctic Oceanology II: The Australian-New Zealand Sector*, *Antarctic Res. Ser.* vol. 19, edited by D. E. Hayes, pp. 125–145, AGU, Washington D. C.

Hayes, D. E., and K. A. Kane (1994), Long-lived mid-ocean ridge segmentation of the Pacific-Antarctic ridge and the Southeast Indian ridge, *J. Geophys. Res.*, *99*, 19,679–19,692.

Holmes, R. C., M. Tolstoy, J. R. Cochran, and J. S. Floyd (2005), Crustal structure along the Southeast Indian Ridge from seismic refraction data, *Eos Trans. AGU*, *86*(52), Fall Meet. Suppl., Abstract T33A-0513.

Kane, K. A., and D. E. Hayes (1994), A new relationship between subsidence rate and zero-age depth, *J. Geophys. Res.*, *99*, 21,759–21,778.

Klein, E. M., and C. H. Langmuir (1987), Global correlations of ocean ridge basalt chemistry with axial depth and crustal thickness, *J. Geophys. Res.*, *92*, 8089–8115.

Klein, E. M., C. H. Langmuir, A. Zindler, H. Staudigel, and B. Hamelin (1988), Isotope evidence of a mantle convection boundary at the, Australian-Antarctic Discordance, *Nature*, *333*, 623–629.

Kojima, Y., M. Shinohara, K. Mochizuki, T. Yamada, K. Nakahigashi, and T. Kanazawa (2003), Seismic velocity structure in the Australian-Antarctic Discordance, Segment B4 revealed by airgun-OBS experiment, *Eos Trans. AGU*, *84*(46), Fall Meet. Suppl., Abstract S21F-0396.

Kuo, B. (1993), Thermal anomalies beneath the Australian-Antarctic Discordance, *Earth Planet. Sci. Lett.*, *119*, 349–364.

Lister, C. R. B. (1977), Estimators for heat flow and deep rock properties based on boundary layer theory, *Tectonophysics*, *41*, 157–171.

Ma, Y., and J. R. Cochran (1997), Bathymetric roughness of the Southeast Indian Ridge: Implications for crustal accretion at intermediate spreading rate mid-ocean ridges, *J. Geophys. Res.*, *102*, 17,697–17,711.

Mahoney, J. J., D. W. Graham, D. M. Christie, K. T. M. Johnson, L. S. Hall, and D. L. Vonderhaar (2002), Between a hotspot and a cold spot; isotopic variation in the Southeast Indian Ridge asthenosphere, 86–118°E, *J. Petrol.*, *43*, 1155–1176.

Marks, K., P. R. Vogt, and S. A. Hall (1990), Residual depth anomalies and the origin of the Australian-Antarctic Discordance, *J. Geophys. Res.*, *95*, 17,325–17,337.

Marks, K. M., J. M. Stock, and K. J. Quinn (1999), Evolution of the Australian-Antarctic Discordance since Miocene time, *J. Geophys. Res.*, *104*, 4967–4982.

Masters, G., G. Laske, H. Bolton, and A. Dziewonski (2000), The relative behavior of shear velocity, bulk sound speed, and compressional velocity in the mantle: Implications for chemical and thermal structure, in *Earth's Deep Interior*, *Geophys. Monogr. Ser.*, vol. 11, edited by S. I. Karato, pp. 763–87, AGU, Washington, D. C.

McKenzie, D. (1967), Some remarks on heat flow and gravity anomalies, *J. Geophys. Res.*, *72*, 6261–6273.
McKenzie, D. (1984), The generation and compaction of partially molten rock, *J. Petrol.*, *25*, 713–765.
McKenzie, D., J. Jackson, and K. Priestley (2005), Thermal structure of oceanic and continental lithosphere, *Earth Planet. Sci. Lett.*, *233*, 337–349.
Megnin, C., and B. R. Romanowicz (2000), The three-dimensional shear velocity structure of the mantle from the inversion of body, surface, and higher mode waveforms, *Geophys. J.*, *143*, 709–728.
Montagner, J.-P. (1986), First results on the 3-dimensional structure of the Indian Ocean inferred from long period surface waves, *Geophys. Res. Lett.*, *13*, 315–318.
Morgan, G. A., H. S. Fleming, and R. H. Feden (1979), Project Investigator-I: A cooperative US/Australian airborne geomagnetic study south of Australia, paper presented at 13th International Symposium on Remote Sensing on Environment, Univ. of Mich., Ann Arbor.
Niu, Y., and R. Batiza (1991), An empirical method for calculating melt compositions produced beneath mid-ocean ridges; for axis and off-axis (seamounts) melting application, *J. Geophys. Res.*, *96*, 21,753–21,777.
Okino, K., K. Matsuda, D. M. Christie, Y. Nogi, and K. Koizumi (2004), Development of oceanic detachment and asymmetric spreading at the Australian-Antarctic Discordance, *Geochem. Geophys. Geosyst.*, *5*, Q12012, doi:10.1029/2004GC000793.
Parsons, B., and J. G. Sclater (1977), An analysis of the variation of ocean floor bathymetry and heat flow with age, *J. Geophys. Res.*, *82*, 803–827.
Patriat, P., and M. Doucouré (1992), Thermal diffusivity of the lithosphere derived from altimetry and bathymetry profiles across the Southwest Indian Ridge, *Geophys. Res. Lett.*, *19*, 1543–1546.
Priestley, K., and D. P. McKenzie (2006), The thermal structure of the lithosphere from shear wave velocities, *Earth Planet. Sci. Lett.*, *244*, 285–301.
Ritsema, J., and H. J. van Heijst (2000), Seismic imaging of structural heterogeneity in Earth's mantle: Evidence for large-scale mantle flow, *Sci. Progr.*, *83*, 243–259.
Ritzwoller, M. H., N. M. Shapiro, and G. M. Leahy (2003), A resolved mantle anomaly as the cause of the Australian-Antarctic Discordance, *J. Geophys. Res.*, *108*(B12), 2559, doi:10.1029/2003JB002522.
Roult, G., D. Rouland, and J.-P. Montagner (1994), Antarctica II: Upper mantle structures from velocities and anisotropy, *Phys. Earth Planet. Inter.*, *84*, 33–57.
Royer, J.-Y., and D. Sandwell (1989), Evolution of the Eastern Indian Ocean since the late Cretaceous: Constraints from Geosat altimetry, *J. Geophys. Res.*, *94*, 13,755–13,782.
Scheirer, D. S., D. W. Forsyth, J. A. Conder, M. A. Eberle, S. Hung, K. T. M. Johnson, and D. W. Graham (2000), Anomalous seafloor spreading of the Southeast Indian Ridge near the Amsterdam-St. Paul Plateau, *J. Geophys. Res.*, *105*, 8243–8262.
Sempéré, J., J. R. Cochran, and SEIR Scientific Team (1997), The Southeast Indian Ridge between 88°E and 118°E: Variations in crustal accretion at constant spreading rate, *J. Geophys. Res.*, *102*, 15,489–15,506.
Shah, A. K., and J. Sempére (1998), Morphology of the transition from an axial high to a rift valley at the Southeast Indian Ridge and the relation to variations in mantle temperature, *J. Geophys. Res.*, *103*, 5203–5224.
Small, C. (1995), Observations of ridge-hotspot interactions in the Southern Ocean, *J. Geophys. Res.*, *100*, 17,931–17,946.
Small, C., J. R. Cochran, J.-C. Sempéré, and D. Christie (1999), The structure of the Southeast Indian Ridge, *Mar. Geol.*, *161*, 1–12.
Smith, W. H. F., and D. T. Sandwell (1997), Global sea floor topography from satellite altimetry and ship depth soundings, *Science*, *277*, 1956–1962.
Su, W., C. Mutter, J. Mutter, and W. R. Buck (1994), Some theoretical predictions on the relationships among spreading rate, mantle temperature, and crustal thickness, *J. Geophys. Res.*, *99*, 3215–3227.
Sykes, J. S. (1995), Paleobathymetry of the Southern Hemisphere, Ph.D. thesis, 139 pp., Univ. of Wales, Cardiff.
Tikku, A., and S. Cande (1999), The oldest magnetic anomalies in the Australian-Antarctic Basin: Are they isochrons?, *J. Geophys. Res.*, *104*, 661–677.
Tolstoy, M., J. R. Cochran, S. M. Carbotte, and J. S. Floyd (2002), Crustal thickness on the Southeast Indian Ridge from OBH data, *Eos Trans. AGU*, *83*(47), Fall Meet. Suppl., Abstract T12B-1314.
Turcotte, D. L., and G. Schubert (1982), *Geodynamics: Applications of Continuum Physics to Geological Problems*, John Wiley, Hoboken, N. J.
Veevers, J. J. (1982), Australian-Antarctic depression from the mid-ocean ridge to adjacent continents, *Nature*, *326*, 315–317.
Vogt, P. R., N. Z. Cherkis, and G. A. Morgan (1983), Project Investigator: Evolution of the Australia-Antarctic Discordance deduced from a detailed aeromagnetic study, in *Antarctic Earth Science*, edited by R. L. Oliver, P. R. James, and J. B. Jago, pp. 608–613, Aust. Acad. of Sci., Canberra.
Weissel, J. K., and D. E. Hayes (1974), The Australian-Antarctic Discordance: New results and implications, *J. Geophys. Res.*, *79*, 2579–2587.
Wessel, P., and W. H. F. Smith (1991), Free software helps map and display data, *Eos Trans. AGU*, *72*, 441.
West, B., J.-C. Sempéré, D. Pyle, J. Phipps-Morgan, and D. Christie (1994), Evidence for variable upper mantle temperature and crustal thickness in and near the Australian-Antarctic Discordance, *Earth Planet. Sci. Lett.*, *128*, 135–153.

D. Christie, West Coast and Polar Regions Undersea Research Center, University of Alaska Fairbanks, P.O. Box 757220, Fairbanks, AK 99775-7220, USA. (dchristie@guru.uaf.edu)

J. R. Cochran, Lamont-Doherty Geological Observatory of Columbia University, 109 Oceanography, Palisades, NY 10964, USA.

C. Fouchet, L. Géli, and C. Labails, Marine Geosciences Department, Ifremer, B.P. 70, F-29280, Plouzané, France. (louis.geli@ifremer.fr)

J. Francheteau, Université de Bretagne Occidentale, UMR CNRS 6538, Place Nicolas Copernic, 29280, Plouzané, France.

T. C. Lee, College of Ocean and Atmospheric Sciences, Oregon State University, Corvallis, OR 97331-5503, USA.